Revue des Energies Renouvelables Vol. 16 N°1 (2013) 91 – 103
DOI: https://doi.org/10.54966/jreen.v16i1.366

Three-level NPC voltage source converter based direct power control of the doubly fed induction generator at low constant switching frequency

Youcef Djeriri [*], Abdelkader Meroufel, Baghdad Belabbes and Ahmed Massoum

Intelligent Control & Electrical Power Systems Laboratory, 'ICEPS'
Department of Electrical Engineering, Engineer Sciences Faculty,
Djillali Liabes University, Sidi Bel-Abbes, 22000, Algeria

(reçu le 10 Juin 2012 – accepté le 29 Mars 2013)

Abstract - *This paper deals with an improvement of the direct power control 'DPC' for three-level voltage source inverter NPC-VSI feeds the rotor of the doubly fed induction generator 'DFIG' based wind power generation system. This converter allows controlling the rotor voltage in magnitude and phase angle with a high flexibility and can therefore be used for active and reactive power control of DFIG. The control is especially designed to reduce the harmonic distortion of the generated currents and active power ripples of the classical DPC control using switching table. In addition, it's convenient for high power drive and variable speed generator applications with constant switching frequency. The detailed operation principle and simulation results of the proposed DPC-NPC strategy for 1.5 MW of DFIG are also discussed.*

Résumé – *Cet article traite de l'amélioration du contrôle de la puissance directe 'DPC' pour trois niveaux de tension de l'onduleur NPC-VSI, alimentant le rotor du générateur asynchrone à double alimentation 'MADA' à base d'énergie éolienne. Ce convertisseur permet de contrôler la tension du rotor en amplitude et en angle de phase avec une grande flexibilité et peut donc être utilisé pour le contrôle de la puissance active et réactive de la 'MADA'. Le contrôle est spécialement conçu pour réduire la distorsion harmonique des courants générés et des ondulations du contrôle de la puissance active 'DPC' classique en utilisant la table de commutation. En outre, il est commode pour des fortes puissances et des générateurs à vitesse variable avec une fréquence de commutation constante. Le principe de fonctionnement détaillé et les résultats de simulation de la stratégie DPC-NPC proposé pour 1,5 MW de la 'MADA' sont également discutés.*

Keywords: Doubly fed induction generator - Direct power control – Three-level NPC - Constant switching frequency.

1. INTRODUCTION

Compared with the fixed speed induction generator used in wind power generation system, doubly fed induction generator, 'DFIG' offers a number of merits such as maximum wind energy capturing, four-quadrant active and reactive power regulation, low converter cost and reduced power losses, all of which make DFIG become the most popular solution for wind energy conversion systems, 'WECS' applications (Fig. 1).

Stator voltage oriented control 'SVOC' or stator flux oriented control 'SFOC' [1, 2] and direct power control 'DPC' [3, 4] are the two most popular control strategies for the grid-side and rotor side converters in a DFIG system. Theoretically, the vector control

[*] Djeriri_youcef@yahoo.fr

provides fault ride-through capability under both balanced [5] and unbalanced grid-fault conditions [6] and has been undergoing significant development. But the complexity of control structure, especially under parameters variations conditions of DFIG, is the main drawback which boosts the demands on the hardware and the robustness of the control system.

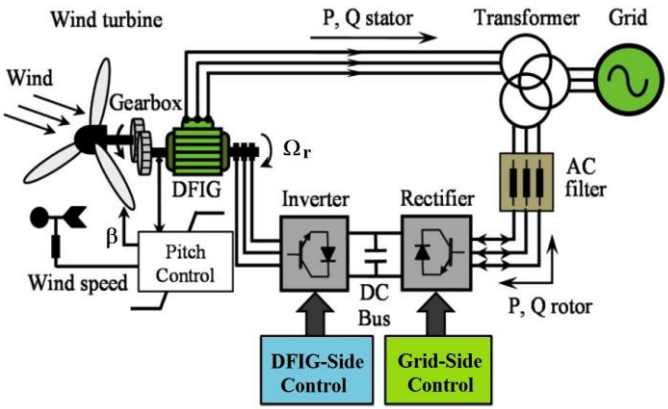

Fig. 1: WECS based doubly fed induction generator

The basic idea of the DPC approach is the direct control of active and reactive power without any internal control loop or PWM modulator. The switching states are selected via a switching table and the states are chosen based on the instantaneous error between the estimation and the desired active and reactive power.

Traditionally, the DPC was investigated for low power applications [7] where normally the standard two-level topology is employed. However, high voltage applied to the semiconductors limits the use of this topology for high power and high voltage applications, an area in which multilevel inverters are emerging.

Since its introduction in 1981 [8], the three-level neutral point clamped, 'NPC' voltage source inverter, 'VSI' has demonstrated some advantages over the conventional two-level inverter. It has been applied in medium and high power applications due to the inherent advantages, namely: voltage across the switches is clamped to half of the dc-link, produces low output voltage and current harmonic distortion.

In this paper, the DPC-NPC strategy is proposed to control a doubly fed induction generator using the three-level voltage source inverter NPC-VSI structure [9, 10]. These converters allow controlling the rotor voltage in magnitude and phase angle and can therefore be used for active and reactive power control.

The control is especially designed to reduce the current harmonics distortion and the powers ripples of the classical DPC strategy using switching table. In addition, it's convenient for high power drive and variable speed generator applications with restricted switching frequency. The detailed operation principle and simulation results of the proposed control strategy are also discussed.

2. WIND TURBINE MODEL

The relation between the wind speed and mechanic power, delivered by the wind turbine, can be described by the following equation:

$$P_t = 1/2 \times \rho \times R^2 \times v^3 \times C_p(\lambda,\beta) \quad (1)$$

$$\lambda = \Omega_r \times R / v \quad (2)$$

where C_p, Power coefficient; λ, Relative speed; β, Pitch angle (deg); R, Radius of turbine; Q_r, Turbine speed (rd/s); v, Wind speed (m/s); ρ, Air density (1.225 kg/m^3).

For the variables speed wind turbines, approximate expression of the power coefficient can be described by the following expression:

$$C_p = f(\lambda,\beta) = C_1 \times \left(\frac{C_2}{\lambda_i} - C_3 \times \beta - C_4 \right) \times \exp\left(\frac{-C_5}{\lambda_i} \right) + C_6 \times \lambda \quad (3)$$

$$\frac{1}{\lambda_i} = \frac{1}{\lambda + 0.08 \times \beta} - \frac{0.035}{\beta^3 + 1} \quad (4)$$

where, $C_1 = 0.5176$; $C_2 = 116$; $C_3 = 0.4$; $C_4 = 5$; $C_5 = 21$; $C_6 = 0.0068$.

The torque produced by the turbine is expressed in the following way:

$$T_t = P_t / \Omega_r = 1/2 \times \rho \times \pi \times R^3 \times v^2 \times C_t(\lambda,\beta) \quad (5)$$

where, C_t is the torque coefficient expressed by:

$$C_t = C_p / \lambda \quad (6)$$

No wind turbine could convert more than 59 % of the kinetic energy of the wind into mechanical energy turning a rotor [11]. This is known as the Betz limit, and it is the theoretical maximum coefficient of power (C_{pmax}) for any wind turbine: $C_{pmax} = 16/27 \approx 0.593$.

In practice, for the good turbines it is in the range of 0.40 to about 0.50. The tip speed ratio (λ) for wind turbines is the ratio between the rotational speed of the tip of a blade and the actual velocity of the wind (Fig. 2).

3. MODELING OF THE DFIG

In the rotating field reference frame of Park, the model of the DFIG is given by the following equations:

Stator voltage components-

$$\begin{cases} V_{ds} = R_s \times I_{ds} + \frac{d}{dt}\Phi_{ds} - \omega_s \times \Phi_{qs} \\ V_{qs} = R_s \times I_{qs} + \frac{d}{dt}\Phi_{qs} + \omega_s \times \Phi_{qs} \end{cases} \quad (7)$$

Rotor components-

$$\begin{cases} V_{dr} = R_r \times I_{dr} + \frac{d}{dt}\Phi_{dr} - (\omega_s - \omega_r) \times \Phi_{qr} \\ V_{qr} = R_r \times I_{qr} + \frac{d}{dt}\Phi_{qr} + (\omega_s - \omega_r) \times \Phi_{dr} \end{cases} \quad (8)$$

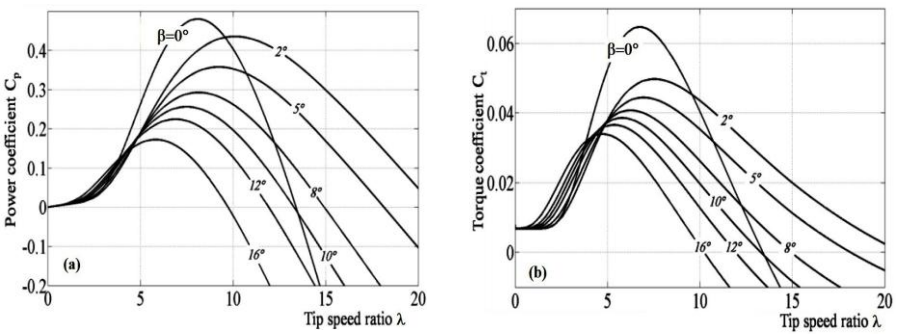

Fig. 2: Pitch angle effect on the aerodynamic coefficient of power (**a**) and on the aerodynamic coefficient of torque (**b**)

Stator flux components-

$$\begin{cases} \Phi_{ds} = L_s \times I_{ds} + L_m \times I_{dr} \\ \Phi_{qs} = L_s \times I_{qs} + L_m \times I_{qr} \end{cases} \tag{9}$$

Rotor flux components-

$$\begin{cases} \Phi_{dr} = L_{rs} \times I_{dr} + L_m \times I_{ds} \\ \Phi_{qr} = L_r \times I_{qr} + L_m \times I_{qs} \end{cases} \tag{10}$$

DFIG electromagnetic torque-

$$T_{em} = -3/2 \times p \times (L_m / L_r) \times (\Phi_{ds} \times I_{qr} - \Phi_{qs} \times I_{dr}) \tag{11}$$

Let us note that this torque represents a disturbance for the wind turbine and takes a negative value.

Mechanical equation-

$$T_t = T_{em} + J \times \frac{d\Omega_r}{dt} + f_r \times \Omega_r \tag{12}$$

Generator active and reactive powers at the grid side are:

$$\begin{cases} P_s = 3/2 \times (V_{ds} \times I_{ds} + V_{qs} \times I_{qs}) \\ Q_s = 3/2 \times (V_{qs} \times I_{ds} - V_{ds} \times I_{qs}) \end{cases} \tag{13}$$

4. DIRECT POWER CONTROL PRINCIPLE

The basic principle of the Direct Power Control, 'DPC' was proposed by Noguchi [7] and is based on the well know Direct Torque Control, 'DTC' for induction machines introduced by Takahashi [12] in the 80s. In the DPC, the active and reactive powers replace the torque and flux amplitude used as the controlled output in the DTC.

The basic concept consists of selecting the appropriate switching states from a switching table based on the errors, which are limited by a hysteresis band, present in the active and reactive powers as illustrated in figure 3.

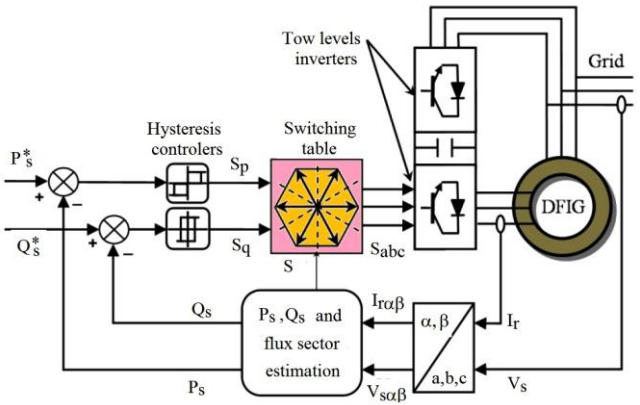

Fig. 3: Schematic diagram of the conventional DPC strategy for DFIG

Instead of measuring the tow powers on the line, we capture the rotor currents, and estimate P_s and Q_s. This approach gives an anticipated control of the powers in the stator windings. By using the stator flux oriented control and the hypothesis of ($R_s = 0$), we can find the relations of P_s and Q_s according to both components of the rotor flux in α, β plane as follows:

$$\begin{cases} P_s = -(3/2) \times \dfrac{L_m}{L_s \times L_r - L_m^2} \times V_s \times \phi_{\beta r} \\ Q_s = (3/2) \times V_s \times \left(\dfrac{L_m}{L_s \times L_r - L_m^2} \times \phi_s - \dfrac{L_m}{L_s \times L_r - L_m^2} \times \phi_{\alpha r} \right) \end{cases} \tag{14}$$

If we introducting the flux power angle δ between stator and rotor flux space vectors, P_s and Q_s become:

$$\begin{cases} P_s = (3/2) \times \dfrac{L_m}{L_s \times L_r - L_m^2} \times \omega_s \times \left|\overline{\phi_s}\right| \times \left|\overline{\phi_r}\right| \times \sin\delta \\ Q_s = (3/2) \times \dfrac{\omega_s}{L_s \times L_r - L_m^2} \times \left|\overline{\phi_s}\right| \times \left(L_r \times \left|\overline{\phi_s}\right| - L_m \times \left|\overline{\phi_r}\right| \times \cos\delta \right) \end{cases} \tag{15}$$

with

$$\begin{cases} \phi_{\alpha r} = \left(L_r - (L_m^2 / L_s) \right) \times I_{\alpha r} + (L_m / L_s) \times \phi_s \\ \phi_{\beta r} = \left(L_r - (L_m^2 / L_s) \right) \times I_{\beta r} \\ \left|\overline{\phi_s}\right| = (\overline{V_s} / \omega_s) \end{cases} \tag{16}$$

As we see in equation (15), these last two expressions show that the stator active and reactive powers can be controlled by modifying the relative angle between the rotor and stator flux space vectors and their amplitudes. This effect is illustrated in the next sections.

5. ROTOR VOLTAGE VECTORS EFFECT ON POWERS

Required information to analyze the rotor voltage vector effect on the stator active and reactive powers can be obtained by equation (15).

Considering that the stator flux space vector amplitude is constant, the stator active and reactive powers only depend on the relative angle between the fluxes ' δ ', and the rotor flux space vector amplitude.

Considering anti clockwise direction of rotation of the flux vectors in the rotor reference frame to be positive, it may be noted that $\overline{\phi_s}$ is ahead $\overline{\phi_r}$ of in motoring mode of operation and $\overline{\phi_s}$ is behind $\overline{\phi_r}$ in generating mode [3]. This is illustrated in figure 4 '**a**- and **b**-' respectively.

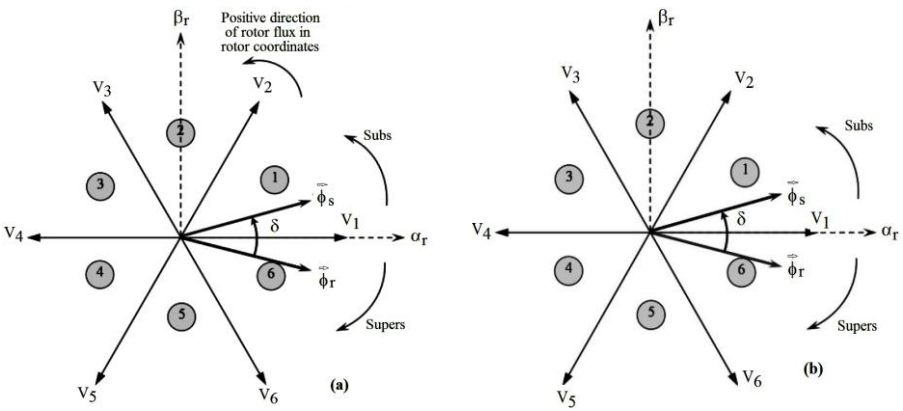

Fig. 4: Flux vectors in rotor coordinates
(**a**) for motoring mode and (**b**) for generating mode

In the rotor reference frame the flux vectors rotate in the positive direction at sub synchronous speeds, remain stationary at synchronous speed and start rotating in the negative direction at super synchronous speeds.

Assuming that the rotor flux is located in the first sector, the application of voltages vectors V_2 and V_3 results in an increase in the stator active power whereas, the application of vectors V_5 and V_6 would reduce it. In the other hand, the application of V_1, V_2 and V_6 would decrease the reactive power drawn from the stator side, while V_3, V_4 and V_5 would increase it.

As a generalization it can therefore, be said that if the rotor flux resides in the K_{th} sector, where $K = 1, 2, \ldots 6$, the application of voltage vectors V_{K+1} and V_{K+2} would increase the delivered stator active power, while the vectors V_{K-1} and V_{K-1} would reduce it. Moreover, the application of V_K, V_{K+1} and V_{K-1} would decrease the delivered reactive power, while V_{K+2}, V_{K-2} and V_{K+3} would increase it. We note that the reactive power control is the same in motor and generator operation modes.

6. DPC SWITCHING TABLE

The references of active and reactive powers values are compared with the estimated ones respectively in hysteresis controllers, with S_p and S_q are the outputs signal of active and reactive powers comparators respectively.

We elaborated the switching table of the control structure; according to the outputs of the controllers S_p, S_q and the rotor flux position δ, such as:

$$\delta = \arctan(\phi_r / \phi_s) \tag{17}$$

For this purpose, the evolution space of $\overline{\phi_r}$ in the considered reference frame is divided into six sectors; this choice is dictated by preoccupation with a more rigorous control, and such as:

$$-\frac{\pi}{6} + (K-1) \times \frac{\pi}{3} \leq \delta(K) \leq \frac{\pi}{6} + (K-1) \times \frac{\pi}{3} \tag{18}$$

with, $K = 1,2,\ldots,6$

The digitized error signal S_p and S_q and the rotor flux sector are input to the swiching table in which every switching state S_a, S_b and S_c of the converter is stored as shown in **Table 1**.

Table 1: Lookup table of the classical DPC

S_q		1			-1		
S_p		**1**	**0**	**-1**	**1**	**0**	**-1**
Flux sector	**1**	V_5	V_7	V_3	V_6	V_0	V_2
	2	V_6	V_0	V_4	V_1	V_7	V_3
	3	V_1	V_7	V_5	V_2	V_0	V_4
	4	V_2	V_0	V_6	V_3	V_7	V_5
	5	V_3	V_7	V_1	V_4	V_0	V_6
	6	V_4	V_0	V_2	V_5	V_7	V_1

7. DPC STRATEGY FOR NPC-VSI

In the Neutral-Point Clamped inverter presented in figure 5, the converter is built around twelve switching cells (based on IGBTs, or others) and six clamp diodes; each phase can produce three distinct levels by connecting the output either to the positive ($v_{DC}/2$), negative ($-v_{DC}/2$) or null (0) potential. In a three phase system it results in $3^3 = 27$ output voltage vectors, related to 19 possible voltage vectors at the output of the converter, (Fig. 6 and **Table 2**).

The output voltage space vector V_r corresponding to the 19 different vectors can be classified into four categories according to its magnitude; it can be summarized in the **Table 2**.

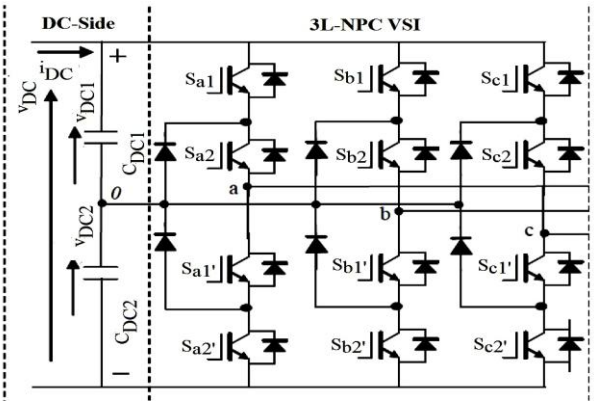

Fig. 5: Three-level NPC voltage source inverter

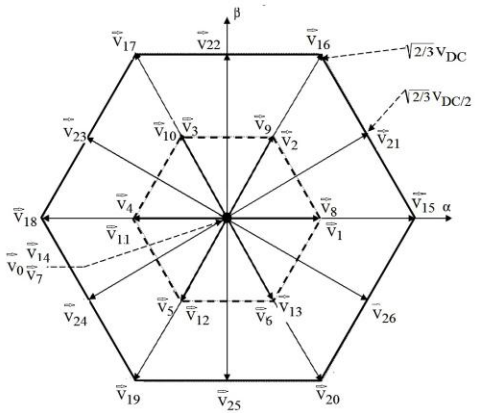

Fig. 6: Space vector diagram of three-level inverter

Table 2: Voltage space vectors generated by the three-level NPC inverter

Zeros Voltages		V_0 (0,0,0)		V_7 (1,1,1)		V_{14} (-1,-1,-1)
Half Voltages	V_1 (1,0,0)	V_2 (1,1,0)	V_3 (0,1,0)	V_4 (0,1,1)	V_5 (0,0,1)	V_6 (1,0,1)
	V_8 (0,-1,-1)	V_9 (0,0,-1)	V_{10} (-1,0,-1)	V_{11} (-1,0,0)	V_{12} (-1,-1,0)	V_{13} (0,-1,0)
Full Voltages	V_{15} (1,-1,-1)	V_{16} (1,1,-1)	V_{17} (-1,1,-1)	V_{18} (-1,1,1)	V_{19} (-1,-1,1)	V_{20} (1,-1,1)
Medium Voltages	V_{21} (1,0,-1)	V_{22} (0,1,-1)	V_{23} (-1,1,0)	V_{24} (-1,0,1)	V_{25} (0,-1,1)	V_{26} (1,-1,0)

So contrary to the two-level inverter which can provide only eight voltage vectors including two null, the 3L-NPC-VSI can produce 27 vectors of voltage including three null (Fig. 6). With 27 possible choices for space vector selection, the Switching Table in three-level inverters becomes more complex comparing with two-level inverters; however it allows much more possibilities for appropriate voltage vector selection to satisfy the commutation condition [10].

8. DPC-NPC SWITCHING TABLE

We elaborated the switching table of the control structure; according to the outputs of the controllers S_p, S_q and the rotor flux position δ, such as:

$$\delta = \arctan(\phi_r / \phi_s) \tag{19}$$

For this purpose, the evolution space of $\overline{\phi_r}$ in the considered reference frame is divided into twelve sectors; this choice is dictated by preoccupation with a more rigorous control, and such as:

$$-\frac{\pi}{12} + (K-1)\times\frac{\pi}{6} \le \delta(K) \le \frac{\pi}{12} + (K-1)\times\frac{\pi}{6} \tag{20}$$

with, $K = 1,2,3,\ldots,12$.

The constitution of the switching table (**Table 3**) is based indeed on the choice of the rotor voltage vector applied to make it possible to increase or decrease the magnitude of the reactive power and the active power value.

Table 3: Switching table for the DPC-NPC strategy

S_q		2		1		0		-1		-2	
S_p		**1**	**-1**	**1**	**-1**	**1**	**-1**	**1**	**-1**	**1**	**-1**
Flux sector	**1**	V_{17}	V_{22}	V_3	V_2	V_0	V_0	V_5	V_{13}	V_{25}	V_{20}
	2	V_{23}	V_{17}	V_4	V_3	V_7	V_7	V_6	V_8	V_{20}	V_{26}
	3	V_{18}	V_{23}	V_{11}	V_{10}	V_{14}	V_{14}	V_{13}	V_1	V_{26}	V_{15}
	4	V_{24}	V_{18}	V_{12}	V_{11}	V_0	V_0	V_8	V_2	V_{15}	V_{21}
	5	V_{19}	V_{24}	V_5	V_4	V_7	V_7	V_1	V_9	V_{21}	V_{16}
	6	V_4	V_0	V_2	V_5	V_7	V_1	V_2	V_{10}	V_{16}	V_{22}
	7	V_{20}	V_{25}	V_{13}	V_{12}	V_0	V_0	V_9	V_3	V_{22}	V_{17}
	8	V_{26}	V_{20}	V_8	V_{13}	V_7	V_7	V_{10}	V_4	V_{17}	V_{23}
	9	V_{15}	V_{26}	V_1	V_6	V_{14}	V_{14}	V_3	V_{11}	V_{23}	V_{18}
	10	V_{21}	V_{15}	V_2	V_1	V_0	V_0	V_4	V_{12}	V_{18}	V_{24}
	11	V_{16}	V_{21}	V_9	V_8	V_7	V_7	V_{11}	V_5	V_{24}	V_{19}
	12	V_{22}	V_{16}	V_{10}	V_9	V_{14}	V_{14}	V_{12}	V_6	V_{19}	V_{25}

9. SIMULATION RESULTS

In this part, simulations are investigated with a 1.5 MW DFIG connected to a 398/690 V grid (Appendix), by using the Matlab/Simulink software. The both control strategies DPC and DPC-NPC are simulated, tested and compared in terms of power reference tracking and current harmonics distortion.

We initial simulation with various active and reactive powers steps in nominal regime of DFIG; this last one it's driven at the supersynchronous speed Ω_r = 1700 rpm. The active power step is changed from -1 MW to -1.5 MW at the instants t = 0.5 s

and again from -1.5 MW to -0.6 MW at the instant t = 1 s; while the reactive power step is changed from 0.6 MVAR to -0.6 MVAR at the instant t = 0.75 s. Simulation results are shown in figure 7.

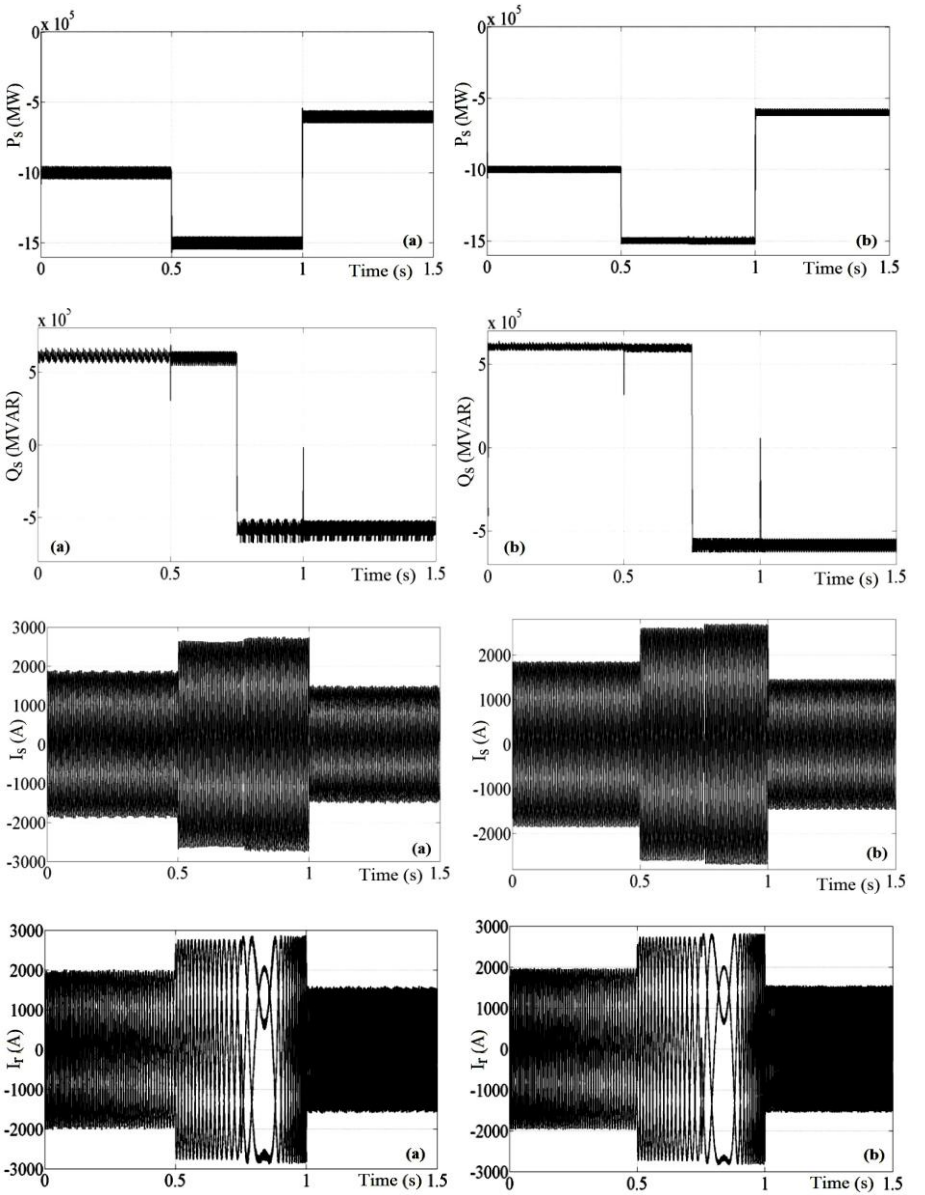

(**a**) DPC strategy (**b**) DPC-NPC strategy

Fig. 7: Simulation results under various stator active and reactive power steps

It can be seen from figure 7 that the tow DPC strategies can control the active and reactive powers of DFIG with a very fast time response without errors under steady-state conditions, the stator and rotor currents wave forms are more close to the suitable sinusoidal signal in the tow cases. However, the ripples in powers are more significant in the case of the classical DPC than in the case of the DPC-NPC.

To observe the effectiveness of the proposed control strategy, 'DPC-NPC' on the reduction of the Total Harmonic Distortion, 'THD' rate of the generated active power and the delivered current at the grid side, we use the Fast Fourier Transform, 'FFT' of the stator current waveform ($I_{s\alpha}$) of the both control strategies; the results are also presented in figure 8.

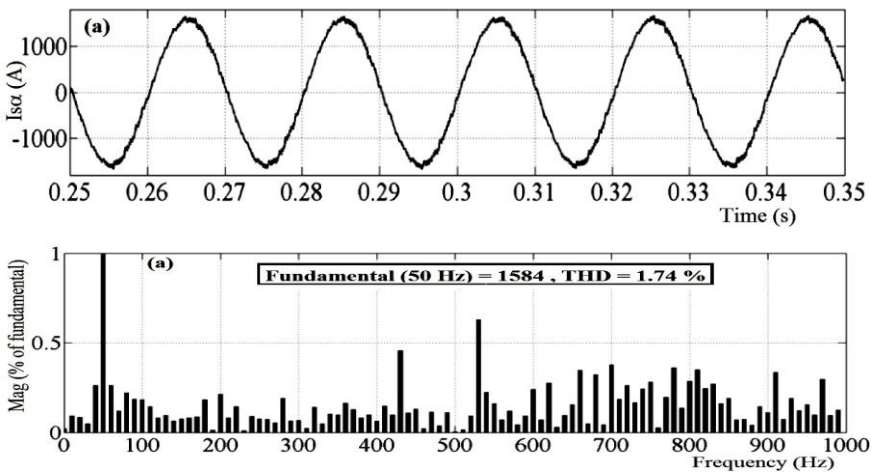

(**a**) Classical DPC

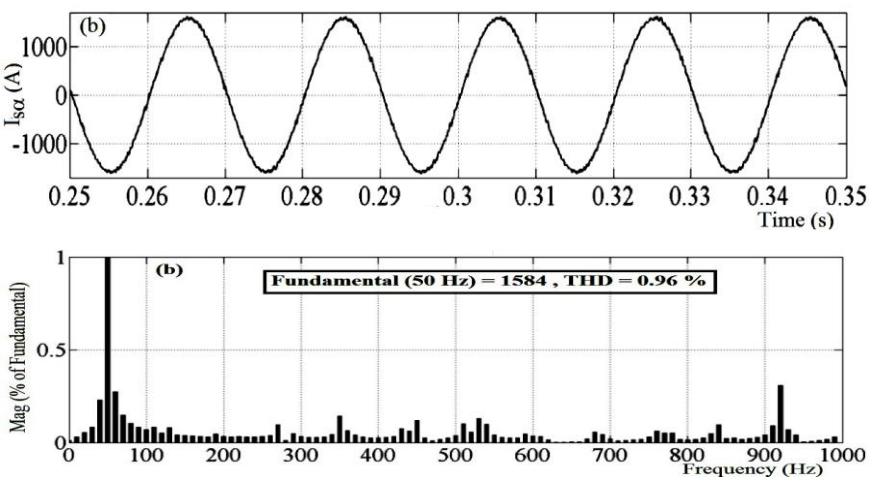

(**b**) DPC-NPC

Fig. 8: THD rate for five cycles starting at t = 0.25 s

A good current wave form is obtained without using any filter for the DPC-NPC scheme, the harmonics in this case are less significant (THD = 0.96%) than those in the case of the classical DPC with the conventional tow-level inverter (THD = 1.74%).

10. CONCLUSION

This paper has presented an improvement of the classical direct power control strategy applied on doubly fed induction generator, when the rotor of this machine is supplied by a three-level NPC inverter. When using a 3L-NPC-VSI topology, the selection of the output voltage vectors becomes more complex due to higher number of available inverter states; however it provides more flexibility for choosing an appropriate voltage vector.

It has been compared by simulation to a DPC strategy based tow-level inverter, '2L-VSI' topology, both strategies showing a similar performance level in steady-state operation. However, the DPC with 2L-VSI presents the drawback to having a high frequency of switching which present a high harmonic distortion of the generated currents at the grid side, high ripples of active and reactive powers of DFIG, and warming-up of the silicon switchers in the inverter.

The proposed DPC-NPC strategy presents good performances, demonstrating that this control technique is an alternative solution to the conventional field oriented control, 'FOC' techniques and presents major improvements with respect to the classical direct power techniques.

APPENDIX

Table 4: Wind turbine parameters

Blade radius, R	35.25 m
Number of blades	3
Gearbox ratio, G	90
Moment of inertia, J	1000 kg.m^2
Viscous friction coefficient, f_r	0.0024 N.m/s
Cut-in wind speed	4 m/s
Cut-out wind speed	25 m/s
Nominal wind speed, v	16 m/s

Table 5: Doubly fed induction generator parameters

Rated power, P_n	1.5 MW
Stator rated voltage, V_s	398/690 V
Rated current, I_n	1900 A
Rated DC-Link voltage, U_{DC}	1200 V
Stator rated frequency, f	50 Hz
Stator inductance, L_s	0.0137 H
Rotor inductance, L_r	0.0136 H
Mutual inductance, L_m	0.0135 H
Stator inductance, R_s	0.012 Ω
Rotor inductance, R_r	0.021 Ω
Number of pair of poles, p	2

REFERENCES

[1] Y. Zhou, P. Bauer, J.A. Ferreira and J. Pierik, '*Control of DFIG Under Unsymmetrical Voltage Dip*', IEEE Power Electronics Specialists Conference, PESC'2007, pp. 933 - 938, 2007.

[2] B. Hopfensperger, D.J. Atkinson and R. Lakin, '*Stator-Flux-Oriented Control of a Doubly-Fed Induction Machine with and without Position Encoder*', IEE Proceedings -Electric Power Applications, vol. 147, N°4, pp. 241 – 250, 2000.

[3] R. Datta and V.T. Ranganathan, '*Direct Power Control of Grid-Connected Wound Rotor Induction Machine without Rotor Position Sensors*', IEEE Transactions Power Electron, Vol. 16, N°3, pp. 390 – 399, 2001.

[4] L. Xu and P. Cartwright, '*Direct Active and Reactive Power Control of DFIG for Wind Energy Generation*', IEEE Transactions Energy Conversion, Vol. 21, N°3, pp. 750 – 758, 2006.

[5] M. Yamamoto and O. Motoyoshi, '*Active and Reactive Power Control for Doubly-Fed Wound Rotor Induction Generator*', IEEE Transactions on Power Electronics, Vol. 6, N°4, pp. 624 – 629, 1991.

[6] J.B. Hu, Y.K. He and L. Xu, '*Dynamic Modeling and Direct Power Control of Wind Turbine Driven DFIG Under Unbalanced Network Voltage Conditions*', Journal of Zhejiang University Science A, Vol. 9, N°12, pp. 1731 – 1740, 2008.

[7] T. Noguchi, H. Tomiki, S. Kondo and I. Takahashi, '*Direct Power Control of PWM Converter without Power Source Voltage Sensors*', IEEE Transactions on Industry Applications, Vol. 34, N°3, pp. 473 – 479, 1998.

[8] A. Nabae, I. Takahashi and H. Akagi, '*A New Neutral Point- Clamped PWM Inverter*', IEEE Transactions on Industry Applications, Vol. IA-17, N°5, pp. 518 - 523, 1981.

[9] G. Abad, M. Á. Rodríguez and J. Poza, '*Three-Level NPC Converter-Based Predictive Direct Power Control of the Doubly Fed Induction Machine at Low Constant Switching Frequency*', IEEE Transactions Industrial Electronics, Vol. 55, N°12, pp. 4419 – 4429, 2008.

[10] L.A. Serpa, S. Ponnaluri, P.M. Barbosa and J.W. Kolar, '*A Modified Direct Power Control Strategy Allowing the Connection of Three-Phase Inverter to the Grid through LCL Filters*', in Proceedings Industry Applications Conference, IAC-05, Vol. 1, pp. 565 – 571, 2005.

[11] E. Hau, '*Wind Turbines*', Springer, 2000.

[12] I. Takahashi and T. Noguchi, '*A New Quick-Response and High-Efficiency Control Strategy of an Induction Motor*', IEEE Transactions on Industry Applications, Vol. IA-22, N°5, pp. 820 – 827, 1986.